J Solid State Electrochem (2011) 15:2587–2592
DOI 10.1007/s10008-010-1254-y

ORIGINAL PAPER

Cobalt oxide–graphene nanocomposite as anode materials for lithium-ion batteries

Guiling Wang · Jincheng Liu · Sheng Tang · Huaiyu Li · Dianxue Cao

Received: 9 October 2010 / Revised: 9 November 2010 / Accepted: 15 November 2010 / Published online: 1 December 2010

Abstract Composites of Co_3O_4/graphene nanosheets are prepared and characterized by X-ray diffraction and scanning electron microscopy. Their electrochemical behavior as anode materials of lithium-ion rechargeable batteries is investigated by galvanostatic discharge/charge measurements and cyclic voltammetry. The composite is composed of Co_3O_4 nanorods (around 20–40 nm in diameter) and nanoparticles (around 10 nm in diameter) distributed within the graphene matrix. The specific capacity of the composite is higher than both Co_3O_4 and graphene nanosheets. The cycling stability of Co_3O_4 is obviously enhanced by compositing with graphene. After 100 cycles, the discharge and charge capacity of the composite is 1,005 and 975 mAh g^{-1}, respectively, and the irreversible capacity loss is less than 3%.

Keywords Cobalt oxide · Graphene nanosheet · Composite · Anode · Lithium-ion battery

Introduction

Nano-sized Co_3O_4 has been demonstrated to be a promising anode material for lithium-ion batteries(LIB) due to its high specific capacity, good cycling and high rate performance [1]. The charge/discharge electrochemical reactions of Co_3O_4 and Li involve the reversible formation and decomposition of Li_2O accompanying by the reduction of Co_3O_4 and the oxidation of Co [1, 2]. This mechanism is different from the insertion/deinsertion mechanism of Li ions for graphite-based intercalation anode materials with layered structures. Co_3O_4 can react with more than eight Li ions per formula, corresponding to a theoretical reversible capacity of 1,100 mAh g^{-1} when discharged to 0 V vs. Li^+/Li [2, 3]. Practical capacities more than 700 mAh g^{-1} have been reported in recent studies for Co_3O_4 nanoparticles, nanowires, nanorods, nanotubes, and hierarchical porous array films [4–12]. These capacities are nearly twice of that of graphite anode currently used in commercial LIB. However, a large specific volume change usually occurs in the Co_3O_4 anode during cycling process due to the pulverization and aggregation of Co_3O_4 particles, which leads to deterioration of electric contact between particles. As a result, Co_3O_4 anode generally exhibited a significant loss of reversible capacity after cycling. Attempts have been made to improve the cycling stability of Co_3O_4 anode by dispersing Co_3O_4 particles on graphitic carbons with high electrical conductivity [7, 10, 13, 14].

Graphene nanosheets (GNS) possess high electrical conductivity, large specific surface area (2,600 m^2g^{-1}) and a broad electrochemical window owing to their unique structure of two-dimensional layers with one-atomic thickness and strongly bonded carbon networks [15–17]. So GNS are promising materials of LIB anode and can also be used as matrices for metal oxides, such as Co_3O_4 and SnO_2. Recently, the performance of GNS as anode materials for rechargeable LIB have been investigated and reversible specific capacities over 600 mAh g^{-1} have been reported [18–20]. The combination of high capacity and relatively good cycling performance of GNS make them of interesting potential candidates of LIB anode materials. Composites of GNS and metal oxides, such SnO_2/GNS and Co_3O_4/NS, have also been investigated as LIB anode material. Their reversible specific capacities are found to be higher than 750 mAh g^{-1} [21–23]. In these composites, GNS efficiently

G. Wang · J. Liu · S. Tang · H. Li · D. Cao (✉)
College of Material Science and Chemical Engineering,
Harbin Engineering University,
Harbin 150001, People's Republic of China
e-mail: caodianxue@hrbeu.edu.cn

buffer the volume change of metal oxides during charge/discharge processes and enhance the electrical conductivity of metal oxides. On the other hand, particles of metal oxides can reduce the degree of stacking of GNS, Which will make GNS retain their high storage capacity of lithium and improve cycling stability. Herein, we reported the preparation of a composite of Co_3O_4/graphite and its electrochemical performance as the anode material of LIB.

Experimental

Preparation of GNS

GNS were synthesized from spherical natural graphite (Qingdao Furunda Graphite Co., Ltd) by a modified Hummers method [24]. Typically, 1 g graphite powder and 0.5 g $NaNO_3$ were added into 70 mL concentrated H_2SO_4 (under ice bath), to which 3 g $KMnO_4$ was gradually added under vigorous stirring condition within 40 min. The mixture was further stirred for another 2 h under ice bath, then warmed up to 40 °C and reacted for 1 h. Seven hundred milliliters of distilled water was slowly added to the mixture to bring the temperature up to 80 °C and maintained at this temperature for 15 min. H_2O_2 (5%) was added into the mixture until the color of the solution turning to brilliant yellow. The obtained powder was collected by filtration, re-dispersed in distilled water and ultrasonicated for 4 h to generate GNS oxides, which were reduced by hydrazine monohydrate under refluxing condition for 2 h. The resulting dark black GNS were dried in a vacuum oven at 80 °C for 10 h to obtain GNS powder.

Preparation and characterization of Co_3O_4/GNS composite

Ten mmol $Co(NO_3)_2$ and 5 mmol NH_4NO_3 were dissolved in 35 mL distilled water to obtain a clear solution, to which 20 mL NH_4H_2O (25 wt.%) was slowly added. White precipitate of $Co(OH)_2$ formed initially and partially turned to reddish brown $Co(OH)_3$ precipitate instantly. With the increase of ammonia, all precipitates re-dissolved to form a clear solution. A mass of 1 g GNS was dispersed into this solution by sonication for 30 min. The suspension was refluxed at 90 °C for 12 h. The solid powder was collected by filtration, dried at 80 °C for 10 h in air, and calcined at 500 °C for 4 h under nitrogen atmosphere to obtain the Co_3O_4/GNS composite. For comparison, pure Co_3O_4 was also prepared as described above.

The morphology was examined by scanning electron microscopy (SEM, JEOL JSM-6480). The structure was analyzed using X-ray diffraction (XRD, Rigaku TTR III) with Cu Kα radiation (λ=0.1514178 nm). The weight content of Co_3O_4 in Co_3O_4/GNS was quantitatively determined by inductively coupled plasma mass spectrometer (ICP-MS, Xseries-II).

Electrochemical measurements

Electrochemical experiments were carried out using two-electrode CR2032 coin type half cells. To make working electrodes, slurries of active materials (Co_3O_4/GNS composite, Co_3O_4 or GNS), carbon black (Ketjenblack EC-600 JD) and poly(vinyl difluoride) (PVDF; weight ratio of 85:8:7) in *N*-methyl-2-pyrrolidone were pasted on pure Cu foil, dried under vacuum at 80 °C for 8 h and pressed at 10 MPa. A Li foil served as the reference and counter electrode. A concentration of 1.0 mol L^{-1} $LiPF_6$ dissolved in a mixture of ethylene carbonate (EC), dimethyl carbonate (DMC) and ethyl methyl carbonate (EMC; volume ratio of 1:1:1) was used as the electrolyte. Microporous polypropene film (Celgard 2400) was used as the separator. The cells were assembled in a nitrogen-filled glove box. The discharge/charge performance was tested at a current density of 74.4 mA g^{-1} in the potential range of 0.0~3.0 V vs. Li^+/Li on a battery test system (CT-3008-5 V/5 mA, Neware Technology Ltd., Shenzhen, China). Cyclic voltammetry (CV) was conducted using an electrochemical workstation (VMP3/Z, Bio-logic, France).

Results and discussion

Structure and morphology of Co_3O_4/GNS composite

Figure 1 shows the XRD patterns of Co_3O_4/GNS composite, Co_3O_4 and GNS. The diffraction peaks of the Co_3O_4 sample are well indexed to the cubic spinel Co_3O_4 (JCPDS card No.

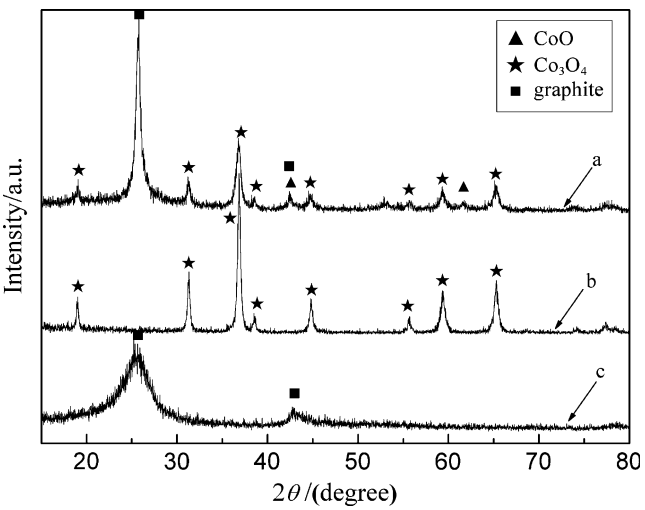

Fig. 1 XRD patterns of Co_3O_4/GNS (**a**), Co_3O_4 (**b**), and GNS (**c**)

42-1467). The XRD pattern of GNS displayed two broad peaks at 25.6° and 42.7°. The main peak at 25.6° corresponding to the (002) plane of graphite occurs at slightly lower angle than that of hexagonal phase graphite (2θ=26.52°, JCPDS card No. 41-1487). The XRD pattern of the Co_3O_4/GNS composite contains all the peaks from Co_3O_4 and the GNS sample. In addition, two minor peaks at 42.4° and 61.6° were observed, which can be attributed to CoO. The peak at 25.6° become sharper and strong comparing with that of GNS sample, implying that restacking of GSN might take place during preparation of the composite. The average size of Co_3O_4 in the composite was estimated to be around 20 nm using the Scherrer's equation based on the peak (311).

Figure 2 shows the SEM image of Co_3O_4 and TEM images of GNS, Co_3O_4/GNS composite. The Co_3O_4 sample was prepared under the same condition as the Co_3O_4/GNS composite in the absence of GNS. The majority of Co_3O_4 are rods with diameters in the nano- and micro-meter range (Fig. 2a). The GNS are crumpled and curved nanosheets (Fig. 2b) with the thickness of around 5 nm (Fig. 2c). In the Co_3O_4/GNS composite, Co_3O_4 presents as nanorods (around 20~40 nm in diameter) and nanoparticles (around 10 nm in diameter; Fig. 2d), and dispersed within GNS matrix. The interaction of Co_3O_4 nanorods with graphene sheets is weaker than that of the nanoparticles with the sheets due to the smaller contact area of nanorods than nanoparticles. Besides, comparing to nanoparticles, nanorods have larger volume expansion/contraction and severer particle aggregation associated with the Li^+ insertion and extraction process. So nanorods might lose their contact during charge/discharge cycling resulting in an irreversible capacity loss and a poor cycling stability. Increasing the interaction force between Co_3O_4 and graphene by controlling the size and shape of Co_3O_4 is expected to enhance the cycling stability of the composite.

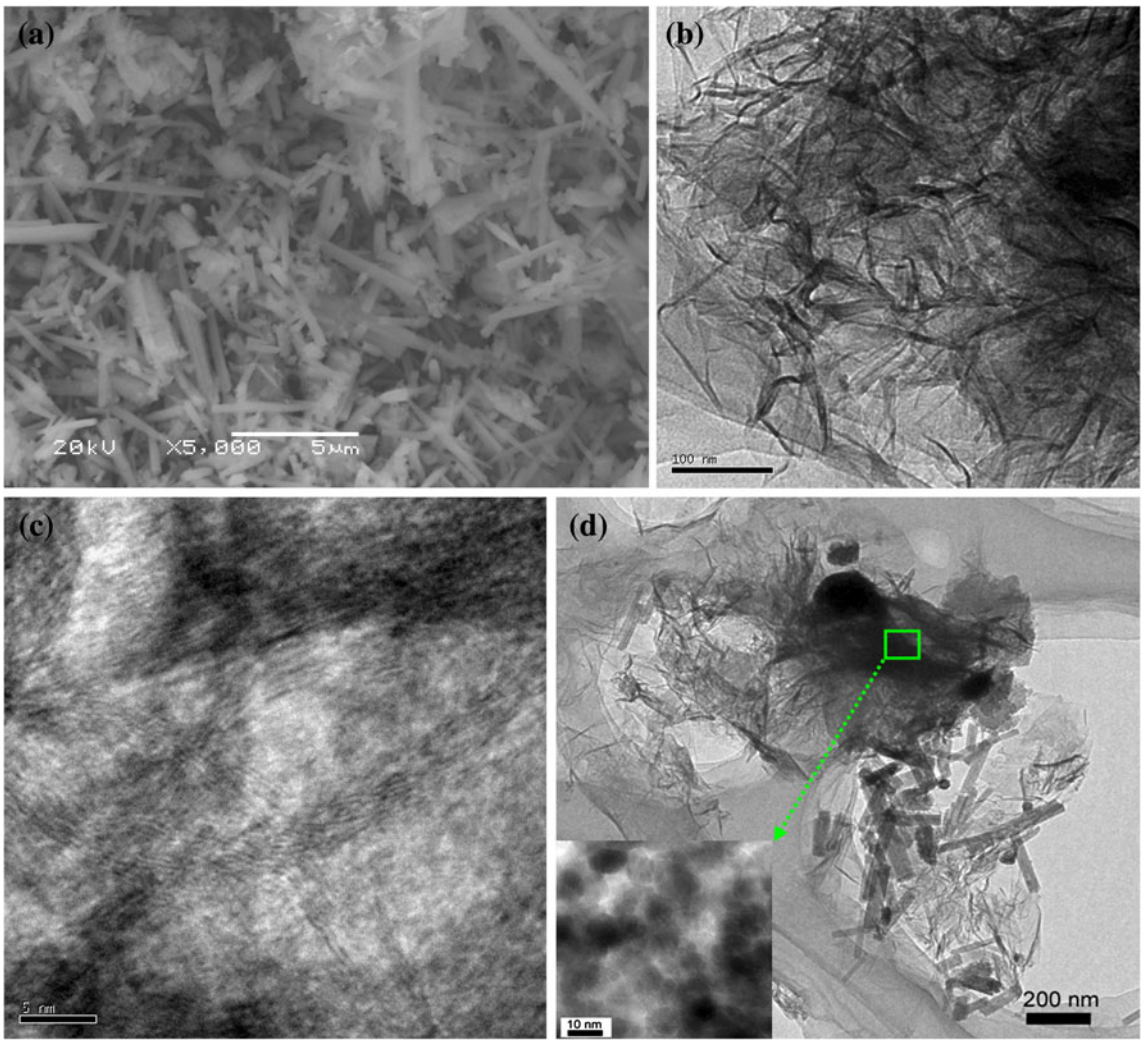

Fig. 2 SEM image of Co_3O_4 (**a**) and TEM images of GNS (**b**, **c**) and Co_3O_4/GNS composite (**d**)

Electrochemical performance of Co_3O_4/GNS composite

Galvanostatic discharge/charge experiments were carried out to evaluate the electrochemical performance of Co_3O_4/graphite composite as the anode material of LIB. For comparison, Co_3O_4 and GNS were also tested under the same conditions. Figure 3a, b and c shows the first three discharge/charge curves of Co_3O_4/GNS composite, Co_3O_4 and GNS, respectively. The curves were measured at a current density of 74.4 mA g^{-1} in the potential range of 0~3.0 V vs. Li^+/Li.

The discharge and charge curves of the three electrodes displayed obviously different behavior. The profile of potential against capacity curves for Co_3O_4 electrode (Fig. 3b) was similar to that of Co_3O_4 nanowires, nanotubes and commercial nanoparticles [4, 5, 10, 22]. The first discharge curve exhibited a distinct potential plateau at about 1.0 V followed by a gradual slope. The potential plateau shifted to around 1.2 V and narrowed in the subsequent discharge curves. This potential plateau corresponds to the reduction of Co_3O_4 to CoO accompanying with the formation of Li_2O. The intermediate of CoO was further converted to Co and Li_2O corresponding to the sloping curve down to the 0.0 V [3, 4, 6, 13]. The total discharge capacity reached 980 mAh g^{-1} in the first cycle, but reduced to 635 mAh g^{-1} after three discharge/charge cycles. The significant loss in capacity is usually attributed to the pulverization and aggregation of Co_3O_4 nanoparticles, which leads to the reduction of electrical contacts between Co_3O_4 nanoparticles and that between Co_3O_4 and current collector. The loss of irreversible capacity is 23% in the first cycle and this value decreases to 12% in the third cycle. This irreversible capacity is mainly attributed to the formation of solid electrolyte interface and the inactivation of part of Li-ion after cycles, which occur primarily in the first cycle.

The discharge/charge behavior of GNS (Fig. 3c) is in good agreement with that reported in the literatures [18–20, 22, 25]. The first discharge curve has a potential plateau at about 0.8 V, which can be attributed to the decomposition of electrolyte and the formation of solid electrolyte interface film. In the subsequent cycles, the discharge/charge curves show a slope without distinguishable plateaus. The absence of plateaus indicated a disordered stacking of GNS resulting in the formation of nonequivalent sites for insertion/deinsertion of Li ions. The discharge and charge capacity are 700 and 550 mAh g^{-1} in the first cycle, corresponding to an irreversible capacity loss of 21%. After three cycles, the discharge capacity decreased to 460 mAh g^{-1}.

The discharge/charge curves of Co_3O_4/GNS composite (Fig. 3a) are obviously different form that of Co_3O_4 and GNS. The curves exhibited combined features of Co_3O_4 (Fig. 3b) and GNS (Fig. 3c). Two potential plateaus at around 1.0 V and 0.5 V in the discharge curves were observed, which can be ascribed to the reduction of Co_3O_4 to CoO and CoO to Co, respectively, as well as the

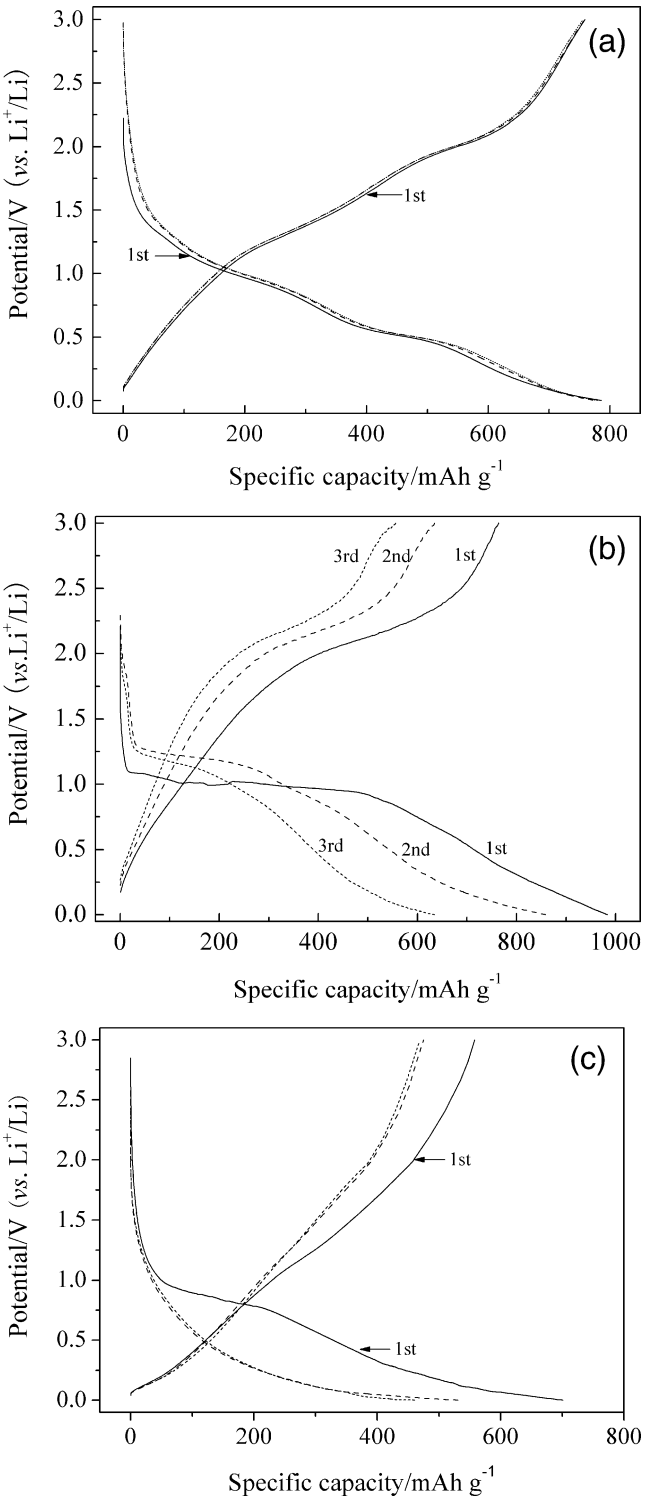

Fig. 3 First three discharge/charge curves of Co_3O_4/GNS composite (**a**), Co_3O_4 (**b**), and GNS (**c**) cycled at a current density of 74.4 mA g^{-1}

insertion of lithium ions into GNS. The plateau at around 1.0 V for the Co_3O_4/GNS is less distinct than that for Co_3O_4. This behavior likely results from GNS in the composite because GNS show no clear potential plateaus (Fig. 3c). It can be concluded that both Co_3O_4 and GNS play active role for storage of lithium ions. More remarkably, the discharge and charge capacities of Co_3O_4/GNS composite remain nearly constant in the initial three cycles. This behavior is very different from that of Co_3O_4 to GNS alone. The discharge and charge capacity is about 780 and 760 mAh g^{-1}, respectively, corresponding to an irreversible capacity loss of 2.5% and a columbic efficiency of 97%. These capacities are larger than that of Co_3O_4 and GNS indicating that there exists a synergistic beneficial effect of Co_3O_4 and GNS. The superior electrochemical performance of Co_3O_4/GNS composite can be attributed to its unique structure. Nano-sized Co_3O_4 in the composite are dispersed within GSN matrix, so volume change and the aggregation of Co_3O_4 during cycling processes might be suppress. Besides, the intimate contact between Co_3O_4 and GNS can significantly decrease the contact resistance of active particles in the composite and thus provide the electrode with a high electrical conductivity. It should be pointed out that the crystalline size of Co_3O_4 in the Co_3O_4/GNS composite is smaller than that of pure Co_3O_4 (Fig. 2a and d). The reduced Co_3O_4 size might also contribute to the enhancement of the capacity and the stability of the composite because it is well known that decreasing the size of Co_3O_4 can shorten the electronic and lithium ion conduction path and reduce the volume change induced by charge and discharge reactions.

The cycling stability of Co_3O_4/GNS composite was further examined by repetitive discharge/charge cycles at a constant current density of 74.4 mA g^{-1}. The results are shown in Fig. 4. The discharge and charge capacity gradually increased within the first 15 cycles and then became relatively stable in the subsequent cycles. After 100 cycles, the discharge and charge capacity are 1,005 and 975 mAh g^{-1}, respectively, corresponding to an irreversible capacity loss of 3%. These results demonstrated that the composite electrode of Co_3O_4/GNS has remarkably good performance and reversibility. In a recent study, Wu et al. [26] investigated a Co_3O_4/GNS composite with the content of Co_3O_4 of 75.4% and found that the composite exhibits a reversible capacity of 935 mAh g^{-1} after 30 cycles at a constant current density of 50 mA g^{-1}. Our Co_3O_4/GNS has lower content of Co_3O_4 and higher specific discharge capacity and better cycling performance than that reported by Wu et al. The difference likely relates to the different Co_3O_4 shape and its content in the composite and dispersion pattern of Co_3O_4 in the composite matrix.

CV measurements were carried out to understand the electrochemical process. Figure 5 shows the cyclic voltammograms of Co_4O_3, GNS, and Co_3O_4/GNS composite electrode at a scan rate of 0.1 mV s^{-1}. For Co_3O_4 electrode, the cyclic voltammogram exhibits two broad reduction peaks at 1.0 V and 2.0 V in the cathodic process and one broad oxidation peak at 2.25 V in the anodic process. This behavior is in good agreements with literature results [9, 10, 12]. It has been reported that the electrochemical reaction mechanism of Li with Co_3O_4 is different from the classical reversible insertion/deinsertion of Li ions in materials with layered structure (e.g., graphite). It involves the formation and decomposition of Li_2O accompanying by the reduction of Co_3O_4 to Co and the oxidation of Co to Co_3O_4 through an intermediate of CoO. This multiple electron process can be represented by Eqs. 1 and 2 [1, 3, 4, 6, 9]. According to this mechanism, the cathodic peak at 2.0 V with low current and at 1.0 V with high current can be ascribed to the reduction of Co_3O_4 and CoO, respectively. The broad

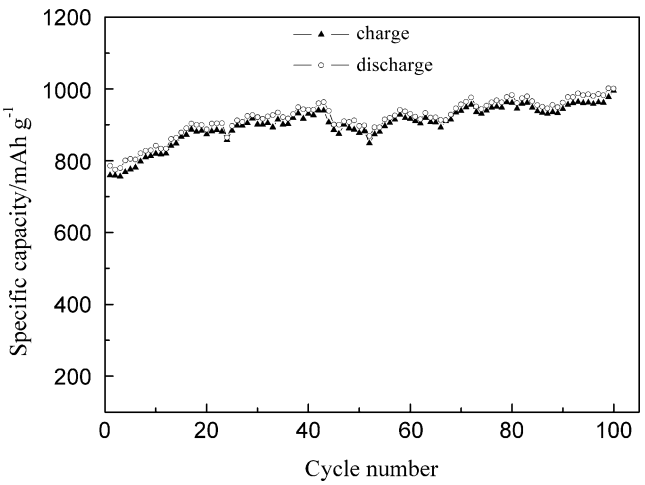

Fig. 4 Cycle performances of Co_3O_4/GNS composite at a current density of 74.4 mA g^{-1}

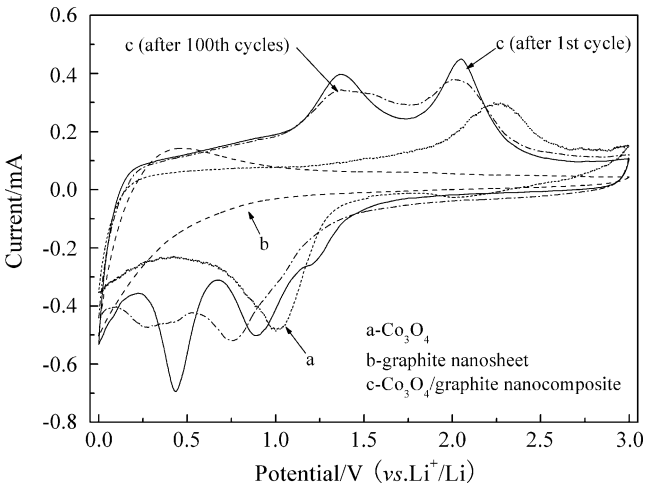

Fig. 5 Cyclic voltammograms of Co_3O_4 (**a**), GNS (**b**) and Co_3O_4/GNS composite (**c**) measured at a scan rate of 0.1 mV s^{-1}

anodic peak starting from around 1.2 V corresponds to the oxidation of metallic Co to CoO and then to Co_3O_4.

$$Co_3O_4 + 2Li^+ + 2e^- \underset{\text{charge}}{\overset{\text{discharge}}{\rightleftharpoons}} Li_2O + 3CoO \quad (1)$$

$$3CoO + 6Li^+ + 6e^- \underset{\text{charge}}{\overset{\text{discharge}}{\rightleftharpoons}} 3Li_2O + 3Co \quad (2)$$

The voltammogram profile of GNS displayed typical feature of graphene reported in literatures [18, 25]. No well-defined cathodic and anodic peaks were observed, which matches well with the discharge/charge profiles without potential plateaus (Fig. 3c). The CV of Co_3O_4/GNS composite exhibited different features from that of Co_3O_4 and GNS. Three cathodic peaks and two anodic peaks were observed in the first cycle. The cathodic peak at 0.43 V significantly reduced after 100 cycles but did not completely disappear. This peak can be attributed to the formation of the solid electrolyte interface membrane and the simultaneous insertion of lithium into graphite nanosheets [18, 25]. The anodic peak at 1.37 V can be assigned to the formation of CoO intermediate [6]. This peak is more visible in the composite electrode than in the Co_3O_4 electrode, which likely results from the decreased particle size and increased electrical conductivity of Co_3O_4 in the composite. Peaks for the reduction of Co_3O_4 and the oxidation of Co in the composite shifted to lower potentials comparing to those for Co_3O_4, an indication of lower resistance of the composite electrode than the Co_3O_4 electrode.

Conclusions

Composites of Co_3O_4/GNS were prepared by simple refluxing of a solution containing $Co(NO_3)_2$,NH_4NO_3 and NH_4H_2O in the presence of graphene nanosheets. The obtained composites exhibit higher specific capacity than both Co_3O_4 and GNS and superior cyclability. The discharge and charge capacities slightly increased within the initial 15 cycles and remained nearly unchanged in the subsequent 85 cycles. The reversible capacity after 100 cycles is 975 mAh g^{-1} with the irreversible capacity loss less than 3%. The high performance of the Co_3O_4/GNS composite can be attributed to the buffer effects of GNS on the volume change and aggregation of Co_3O_4 during cycling processes as well as the reduction of contact resistance of Co_3O_4 particles.

Acknowledgments We gratefully acknowledge the financial support of this research by National Nature Science Foundation of China (20973048), Heilongjiang Postdoc Foundation (LBH-Q06091), Harbin Science and Technology Fund for Young Scholars (2007RFQXG023), Key Laboratory of Superlight Materials and Surface Technology of Ministry of Education.

References

1. Poizot P, Laruelle S, Grugeon S, Dupont L, Tarascon JM (2000) Nature 407:496–499
2. Poizot P, Laruelle S, Grugeon S, Tarascon J-M (2002) J Electrochem Soc 149:A1212–A1217
3. Larcher D, Sudant G, Leriche J-B, Chabre Y, Tarascon J-M (2002) J Electrochem Soc 149:A234–A241
4. Li Y, Tan B, Wu Y (2008) Nano Lett 8:265–270
5. Nam KT, Kim D-W, Yoo PJ, Chiang C-Y, Meethong N, Hammond PT, Chiang Y-M, Belcher AM (2006) Science 312:885–888
6. Xia XH, Tu JP, Xiang JY, Huang XH, Wang XL, Zhao XB (2010) J Power Sources 195:2014–2022
7. Liu HJ, Bo SH, Cui WJ, Li F, Wang CX, Xia YY (2008) Electrochim Acta 53:6497–6503
8. Vidal-Abarca C, Lavela P, Tirado JL (2008) Electrochem Solid-State Lett 11:A198–A201
9. Li WY, Xu LN, Chen J (2005) Adv Funct Mater 15:851–857
10. Du N, Zhang H, Chen BD, Wu JB, Ma XY, Liu ZH, Zhang YQ, Yang DR, Huang XH, Tu JP (2007) Adv Mater 19:4505–4509
11. Lou XW, Deng D, Lee JY, Feng J, Archer LA (2008) Adv Mater 20:258–262
12. Yao W, Yang J, Wang J, Nuli Y (2008) J Electrochem Soc 155: A903–A908
13. Yang R, Wang Z, Liu J, Chen L (2004) Electrochem Solid-State Lett 7:A496–A499
14. Zhi L, Hu YS, Hamaoui BE, Wang X, Lieberwirth I, Kolb U, Maier J, Mulen K (2008) Adv Mater 20:1727–1731
15. Rao CNR, Sood AK, Subrahmanyam KS, Govindaraj A (2009) Angew Chem Int Ed 48:7752–7777
16. Geim AK (2009) Science 324:1530–1534
17. Allen MJ, Tung VC, Kaner RB (2009) Chem Rev 110:132–145
18. Wang G, Shen X, Yao J, Park J (2009) Carbon 47:2049–2053
19. Yoo E, Kim J, Hosono E, Zhou H-S, Kudo T, Honma I (2008) Nano Lett 8:2277–2282
20. Guo P, Song H, Chen X (2009) Electrochem Commun 11:1320–1324
21. Yao J, Shen X, Wang B, Liu H, Wang G (2009) Electrochem Commun 11:1849–1852
22. Yang S, Cui G, Pang S, Cao Q, Kolb U, Feng X, Maier J, Mullen K (2010) ChemSusChem 3:236–239
23. Paek S-M, Yoo E, Honma I (2008) Nano Lett 9:72–75
24. Hummers WS, Offeman RE (1958) J Am Chem Soc 80:1339–1339
25. Lian P, Zhu X, Liang S, Li Z, Yang W, Wang H (2010) Electrochim Acta 55:3909–3914
26. Wu Z, Ren W, Wen L, Gao L, Zhao J, Chen Z, Zhou G, Li F, Cheng H (2010) ACS Nano 4:3187–3194